

4. B. J. Poesz *et al.*, *Proc. Natl. Acad. Sci. U.S.A.* **77**, 7415 (1980).
5. M. Essex *et al.*, *Science* **220**, 859 (1983).
6. R. C. Gallo *et al.*, *ibid.*, p. 865; E. P. Gelmann *et al.*, *ibid.*, p. 862.
7. R. C. Gallo *et al.*, *Cancer Res.* **43**, 3892 (1983); M. G. Robert-Guroff *et al.*, *Science* **215**, 975 (1982).
8. T. H. Lee, C. Howe, M. F. McLane, N. Tachibana, M. Essex, *Leuk. Rev.* **1**, 294 (1983); N. Tachibana *et al.*, in preparation.
9. T. Uchiyama, J. Yodoi, K. Sagawa, K. Takatsuki, H. Uchino, *Blood* **50**, 481 (1977).
10. J. W. Curran, B. L. Evatt, D. N. Lawrence, *Ann. Intern. Med.* **98**, 401 (1983); G. C. White III and H. R. Lesesne, *ibid.*, p. 403.
11. U. K. Laemmli, *Nature (London)* **227**, 680 (1970).
12. Supported in part by grants RD-173 from the American Cancer Society and CA 18216 from the National Institutes of Health. T.H.L. is supported by Institutional Research Service Award 2-T32-CA09031. M.-C. Poon is now located at Foothill Hospital, Calgary, Alberta, Canada. We thank R. Gallo for the reference goat antiserum to HTLV p24.

15 August 1983

Is the Gramicidin A Transmembrane Channel Single-Stranded or Double-Stranded Helix? A Simple Unequivocal Determination

Abstract. *Thallium ion-induced carbonyl carbon chemical shifts were compared for all of the L-residue-peptide carbonyl carbons of the gramicidin A transmembrane channel. Molecular structures were deduced by using the argument that helically equivalent and equally proximal carbonyls would exhibit essentially equivalent ion-induced chemical shifts. The transmembrane channel was found to be a head-to-head dimer with the structure of a left-handed, single-stranded β -helix.*

It is well-accepted that the gramicidin transmembrane channel is a dimer (1-6). However, actively concerned research groups differ in their opinions about the structure of the ion-conducting dimer (7-13): is the structure one of single-stranded helices dimerized end to end, or is it a double-stranded helix? The gramicidin channel was the first ion-selective transmembrane channel to be characterized. Knowledge of the channel structure and ionic mechanism provides an understanding of lipid membrane permeation in terms of the basis for selectivity between anions and cations, between monovalent and divalent ions, and among monovalent ions; it provides fundamental information on the repulsion between ions at fixed distances and the relative solvation power of peptide carbonyls and water; it demonstrates that in the selective passage of ions through a channel the largely dehydrated ion is used, and it shows the relative importance of lipid (positive image force) and partial dehydration barriers to passage through the lipid bilayer. Unambiguous data presented in this report exclude double-stranded helices as possible structures of gramicidin in phospholipid and further identify the ion-binding sites within the channel. These data, when combined with previous results on the same system, demonstrate that the channel is specifically the left-handed, single-stranded β -helix, dimerized head to head.

The approach involves eight separate syntheses of gramicidin A. In each synthesis, one different L-residue carbonyl is 90 percent enriched with carbon-13. The eight syntheses are required in order

that each L-residue carbonyl can be used as a reporter group. The relevant principle is that structurally equivalent, symmetry-related carbonyl carbon nuclei in a helix exhibit essentially the same sensitivity to ion occupancy within the helix. Accordingly, an ion-induced chemical shift exhibited by one carbonyl must also be exhibited by a symmetry-related

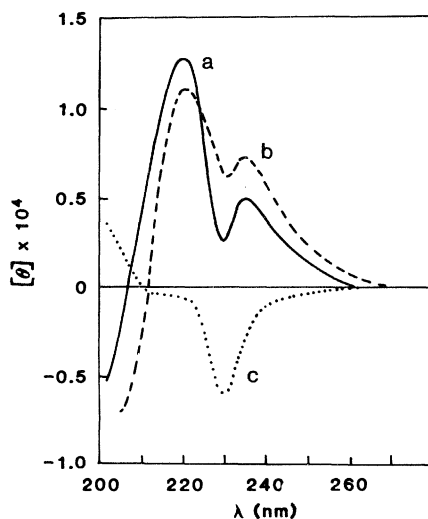


Fig. 1. Unique circular dichroism spectrum of gramicidin A incorporated into lysolecithin membranes, and the effect of thallium ion binding. The molar ratio of gramicidin A to lysolecithin was 1:15. (Curve a) The channel reference spectrum with 0.5 mM NaCl; (curve b) effect of 83 mM thallium acetate; (curve c) the circular dichroism spectrum of gramicidin A in association with lysolecithin micelles before heat incorporation results in the formation of gramicidin-lysolecithin bilayers (18). Incorporation results in a unique circular dichroism spectrum which is only slightly perturbed by thallium ion binding; $[\theta]$, mean molar residue ellipticity; λ , wavelength.

(symmetrically equivalent) carbonyl that is equally proximal to the ion. The present communication is a report of thallium ion-induced carbonyl carbon chemical shifts for $[(1-^{13}\text{C})\text{L-Val}^1]\text{gramicidin A}$, $[(1-^{13}\text{C})\text{L-Ala}^3]\text{gramicidin A}$, $[(1-^{13}\text{C})\text{L-Ala}^5]\text{gramicidin A}$, and $[(1-^{13}\text{C})\text{L-Val}^7]\text{gramicidin A}$. These results combine with previously determined (11) thallium ion-induced carbonyl carbon chemical shifts of $[(1-^{13}\text{C})\text{L-Trp}^9]\text{gramicidin A}$, $[(1-^{13}\text{C})\text{L-Trp}^{11}]\text{gramicidin A}$, $[(1-^{13}\text{C})\text{L-Trp}^{13}]\text{gramicidin A}$, and $[(1-^{13}\text{C})\text{L-Trp}^{15}]\text{gramicidin A}$ to define the helical structure required by the data.

The primary structure of gramicidin A is $\text{HCO-L-Val}^1\text{-Gly}^2\text{-L-Ala}^3\text{-D-Leu}^4\text{-L-Ala}^5\text{-D-Val}^6\text{-L-Val}^7\text{-D-Val}^8\text{-L-Trp}^9\text{-D-Leu}^{10}\text{-L-Trp}^{11}\text{-D-Leu}^{12}\text{-L-Trp}^{13}\text{-D-Leu}^{14}\text{-L-Trp}^{15}\text{-NHCH}_2\text{CH}_2\text{OH}$ as shown by Sarges and Witkop (14). The carbonyl carbons of the L-residues at positions 1, 3, 5, and 7 were labeled with carbon-13, and the synthetic gramicidins were produced as reported for $[(1-^{13}\text{C})\text{D-Leu}^{12,14}]\text{gramicidin A}$ (15). The syntheses of gramicidin A's with labeled carbonyl carbons in L-residues 9, 11, 13, and 15 was verified (16). Each gramicidin A was separately incorporated into lysolecithin phospholipid structures (17). This heat-induced incorporation results in the formation of bilayer sheets and vesicles (18). The evidence that this system contains the channel state is extensive. During the many-hour time course of heat incorporation of gramicidin A into the phospholipid, the motions of the lipid aliphatic carbons become slowed, and a unique circular dichroism pattern develops (Fig. 1). Until the unique circular dichroism pattern is obtained, there is little sodium-23 interaction as measured by nuclear magnetic resonance (NMR) longitudinal (T_1) and transverse (T_2) relaxation studies. The ion interaction that does develop is competitively blocked by silver ion and thallium ion (17, 19), which competitively block alkali metal ion transport through the channel (20, 21). The energy of activation for sodium-23 interaction (17, 19, 22) and for channel transport of sodium ion are essentially the same (23). The interaction of the lysolecithin-packaged gramicidin A with Ca^{2+} and Ba^{2+} has the same binding constants (1 to 10M^{-1}) (24, 25) as were determined from the effect of these divalent ions on channel transport (26). Four rate constants determined by sodium-23 NMR resonance T_1 and T_2 studies can be used with Eyring rate theory to calculate the sodium ion currents through the channel over substantial ranges of ion activity (three decades) and of trans-

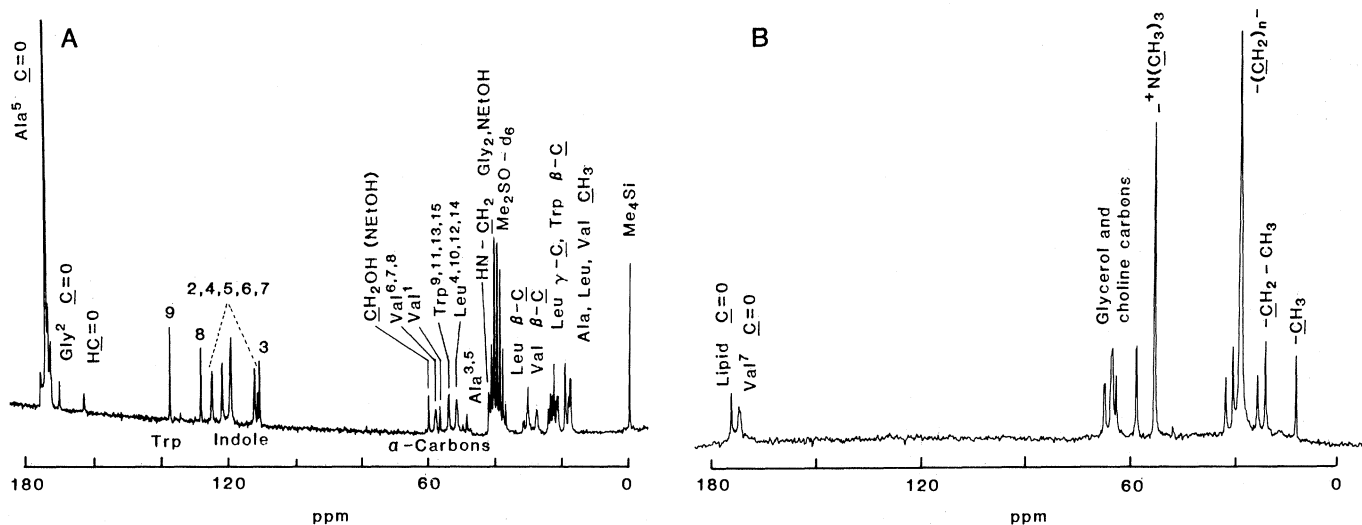


Fig. 2. Carbon-13 nuclear magnetic resonance spectrum (25 MHz) of (A) [(1-¹³C)L-Ala⁵]gramicidin A in dimethylsulfoxide. (B) [(1-¹³C)L-Val⁷]Gramicidin A incorporated into lysolecithin-gramicidin bilayer sheets (18).

membrane potential (50, 100, 150, and 200 mV) (22, 27). Furthermore, the unique circular dichroism pattern (Fig. 1) is the same as that obtained for lecithin membranes (28, 29) and has in that system been defined as the channel state on the basis of the circular dichroism pattern in lecithin of active and nonactive derivatives of gramicidin A (29). Thus, it can be concluded that the channel state is obtained in this system.

Carbon-13 NMR spectra of the (1-¹³C)-enriched gramicidins were measured at 25 MHz on a spectrometer (JEOL FX-100) equipped with a 10-mm multinuclear probe under conditions of complete proton noise decoupling. A representative spectrum of synthetic [(1-¹³C)L-Ala⁵]gramicidin A in dimethylsulfoxide is given in Fig. 2A, where all resonances are assigned and the enriched carbonyl carbon resonance is seen as the intense signal at 172.2 ppm. Each synthetic gramicidin was packaged into lysolecithin structures in ²H₂O at 0.5 mM NaCl (17). In each case, the ion-interacting channel state was verified by circular dichroism spectra, as shown in Fig. 1, and by the sodium-23 NMR chemical shift at 30°C. The concentration of incorporated channels was determined by ultraviolet spectrophotometry and found to be approximately 3 mM for all samples. Ions were introduced to the samples by adding dry thallium acetate or BaCl₂ · 2H₂O salts to the NMR tube.

The spectra of lysolecithin-packaged gramicidins were accumulated at 70°C to facilitate observation of the broad signal of the peptide with the labeled carbonyl carbon. A representative spectrum of the phospholipid-packaged channel may be seen in Fig. 2B where the enriched car-

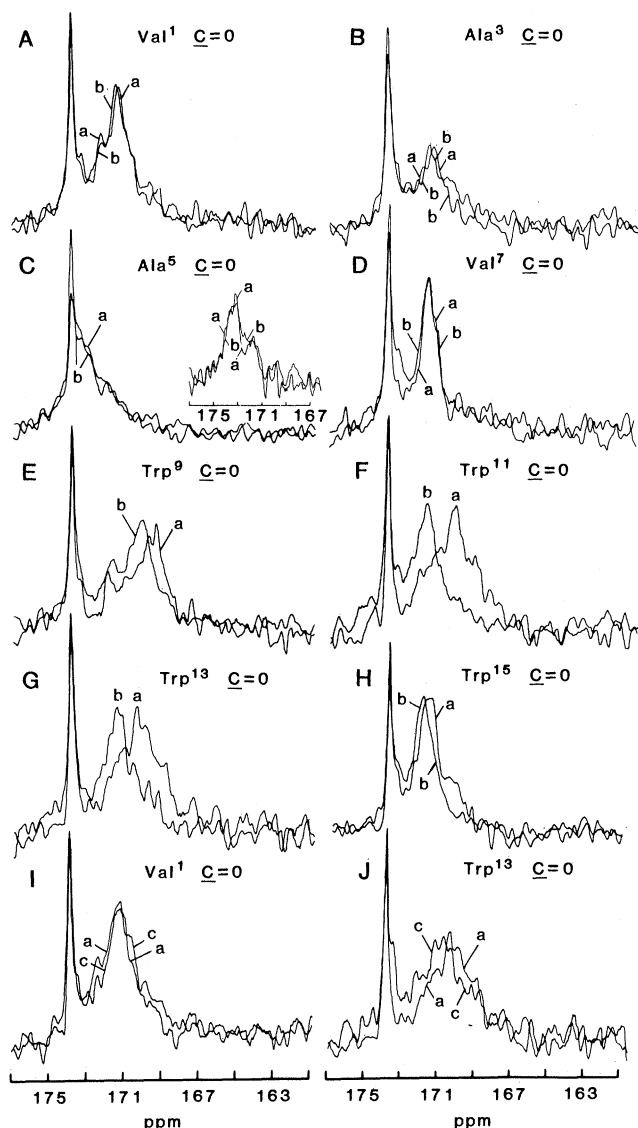


Fig. 3. Carbonyl region of carbon-13 NMR spectra of (1-¹³C)-enriched gramicidin A molecules incorporated into lysolecithin-gramicidin A bilayers (18). (A) [(1-¹³C)L-Val¹]Gramicidin A; (B) [(1-¹³C)L-Ala³]gramicidin A; (C) [(1-¹³C)L-Ala⁵]gramicidin A (inset shows resonance of L-Ala⁵ carbonyl after removal of lipid carbonyl resonance); (D) [(1-¹³C)L-Val⁷]gramicidin A; (E) [(1-¹³C)L-Trp⁹]gramicidin A; (F) [(1-¹³C)L-Trp¹¹]gramicidin A; (G) [(1-¹³C)L-Trp¹³]gramicidin A; (H) [(1-¹³C)L-Trp¹⁵]gramicidin A; (I) [(1-¹³C)L-Val¹]gramicidin A; and (J) [(1-¹³C)L-Trp¹³]gramicidin A. Spectra I and J show the ion-induced carbonyl carbon chemical shift due to 1M BaCl₂. Although barium ion does not pass through the channel, it does interact with the ethanolamine end of the structure, inducing chemical shifts in carbonyls of residues 9, 11, 13, 14, and 15; but it does not perturb the formyl end as monitored with the L-Val¹ carbonyl carbon. This indicates accessibility of the

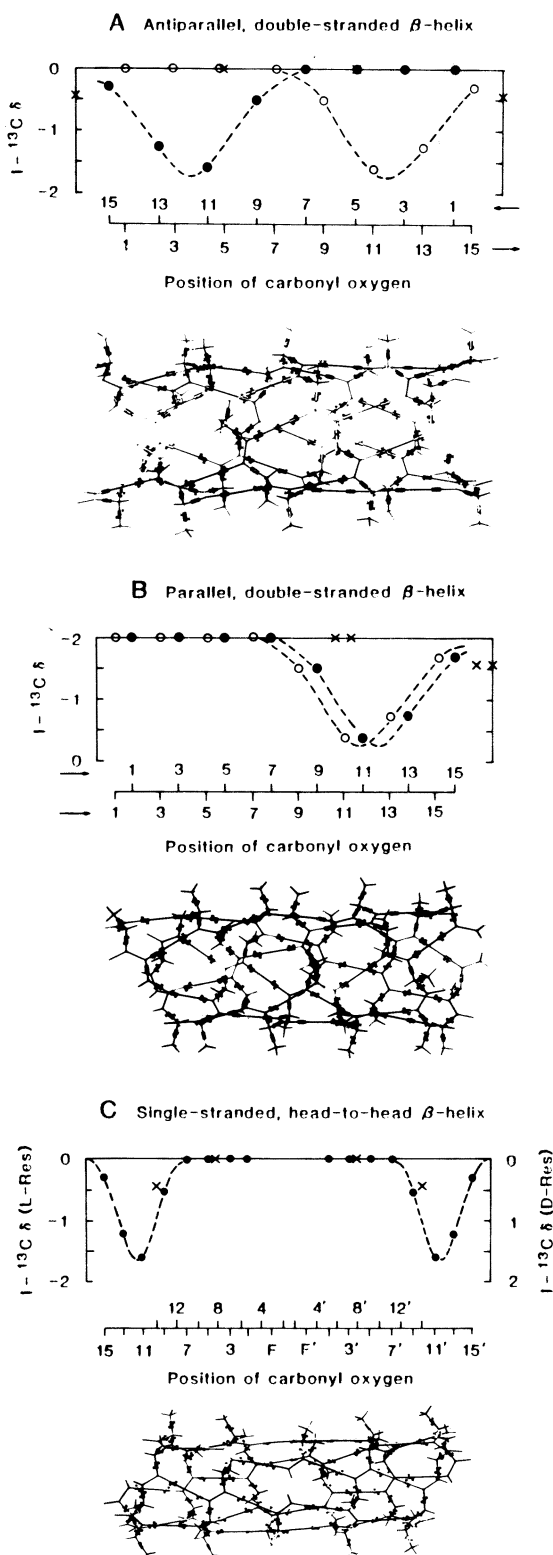
ethanolamine end only to the aqueous interface. Spectra A through E show the chemical shift induced by thallium ion. These values are listed in Table 1 and used in the plots in Fig. 4. (Curves a) 0.5 mM NaCl; (curves b) 83 mM thallium acetate; (curves c) 1M BaCl₂. As reported earlier (11), residues 9, 11, 13, and 15 exhibit chemical shifts, but residues 1, 3, 5, and 7 exhibit no thallium ion-induced chemical shift under identical conditions.

Table 1. Peptide carbonyl carbon chemical shifts for lysolecithin-packaged ($1\text{-}^{13}\text{C}$)-enriched gramicidin A. The chemical shift (δ), in parts per million, was measured with respect to the lysolecithin $-(\text{CH}_2)_n-$ resonance at 29.1 ppm from external hexamethyldisiloxane.

Condition	δ (ppm)							
	Val ¹	Ala ³	Ala ⁵	Val ⁷	Trp ⁹	Trp ¹¹	Trp ¹³	Trp ¹⁵
+0.5 mM Na ⁺	171.4	171.6	173.1	171.7	169.5	170.3	170.1	171.9
+83 mM Tl ⁺	171.4	171.6	173.1	171.7	170.0	171.9	171.3	172.2
Δ^*	0	0	0	0	0.5	1.6	1.2	0.3

*The error is less than 0.1 ppm as determined by multiple incorporations and spectral characterization.

Fig. 4. Wire models of possible channel structures aligned with an abscissa for placing the experimental ion-induced chemical shifts of each of the L-residue carbonyl carbons. (A) Antiparallel, double-stranded β -helix, showing the contradiction with the structure that while residues 9, 11, 13, and 15 exhibit ion-induced chemical shifts, equally proximal and helically equivalent carbonyl carbons of residues 1, 3, 5, and 7 do not exhibit ion-induced chemical shifts. Therefore, this cannot be the structure. (B) Parallel, double-stranded β -helix showing an asymmetric ion binding pattern. This is inconsistent with the symmetric single-channel current-voltage curves, with the demonstration of two ion-binding sites, with the exposed ends of the structure to the aqueous interface and with D-residue 8 and 14 thallium ion-induced carbonyl carbon chemical shifts indicated as X on the plots (see text for further discussion). This structure also cannot be the dominant functional channel. (C) Single-stranded β -helical channel. Thallium ion-induced carbonyl carbon chemical shifts plotted from the data in Fig. 3 and Table 1 for the left-handed, single-stranded $\beta_{3,3}^{6,3}$ -helix of gramicidin A. There are two binding sites, related by a two-fold symmetry axis perpendicular to the channel axis which would give rise to symmetric single-channel current-voltage curves (30, 31) and which are consistent with the sodium-23 NMR studies showing two binding sites (22, 27). The formyl end is buried, and the ethanolamine end is at the aqueous interface; this is consistent with the data of Fig. 3, I and J, and (10). The left-handed helical sense is demonstrated by the thallium ion-induced carbonyl carbon chemical shifts of D-residues 8 and 14 (12). These data are included as the X's. This structure is therefore deducible entirely on the basis of ion-induced carbonyl carbon chemical shifts to be the channel structure.



bonyl carbon of residue 7 is seen as the signal just upfield from the lipid carbonyl resonance. Chemical shifts for all lipid incorporated spectra are given with respect to the fatty acid $-(\text{CH}_2)_n-$ at 29.1 ppm from external hexamethyldisiloxane. The change in chemical shift of the enriched gramicidin carbonyl carbon on addition of ion was measured by overlaying reference spectra (0.5 mM NaCl) with spectra obtained in the presence of 83 mM Tl⁺ or 1M Ba²⁺ so that the line shapes of the enriched peptide carbonyl resonances were superimposed. The chemical shift was then measured as the difference in the sharp lipid carbonyl carbon resonances, which did not in all cases exhibit a change in chemical shift on addition of ion. In the case of the $[(1\text{-}^{13}\text{C})\text{L-Ala}^5]$ gramicidin A, where the peptide and the lipid carbonyl carbon resonances overlap, a spectrum of lysolecithin-packaged natural-abundance ^{13}C -labeled gramicidin A was subtracted from the spectrum of the enriched sample in order that the $[(1\text{-}^{13}\text{C})\text{L-Ala}^5]$ carbonyl carbon might be resolved (see inset in Fig. 3C).

Carbon-13 NMR spectra of the carbonyl regions for each of the L-residue carbonyl carbons are given in Fig. 3. Parts A through D of Fig. 3 are the data for the carbonyl carbon resonances of L-residues 1, 3, 5, and 7; these show no thallium ion-induced chemical shift on addition of 83 mM Tl⁺. In contrast, as shown in parts E through H of Fig. 3, the carbonyls of L-residues 9, 11, 13, and 15 show large chemical shifts. The chemical shifts of these helically equivalent L-residue carbonyls are all given in Table 1. The values may now be plotted for double- and single-stranded β -helices. In Fig. 4A, an assumed antiparallel double-stranded $\beta^{7,2}$ -helix is shown in a wire model with the carbonyl oxygens aligned along the abscissa above. A plot of the thallium ion-induced chemical shifts demonstrates the contradiction that the peptide carbonyls of residues 11 and 13 show large chemical shifts, near 1.5 ppm, whereas the helically equivalent peptide carbonyls of residues 3 and 5, which reside in the same segment of helix, show no significant chemical shift. This contradiction applies regardless of the number of residues per turn in the double-stranded helix. Accordingly, the antiparallel double-stranded β -helix cannot be the channel structure.

In Fig. 4B is shown the wire model of a parallel double-stranded β -helix and above it are plotted the thallium ion-induced carbonyl carbon chemical shifts. These data require a single binding site in the ethanolamine half of the helix. On

the contrary, two binding sites with different binding constants have been observed for the binding of Na^+ to this channel state (27), and as shown in parts I and J of Fig. 3, only the ethanolamine end is accessible to Ba^{2+} interaction, indicating that the formyl end cannot be at the aqueous interface as required for the parallel double-stranded helix. Additionally, such an asymmetric binding would give rise to asymmetric single-channel current-voltage curves (30), whereas the dominant state of the channel exhibits single-channel current-voltage curves that are symmetric (31). In lecithin vesicles with an identical circular dichroism pattern, it has been shown by Weinstein *et al.* (10) that the formyl end is buried in the lipid and not accessible at the aqueous interface. Finally, data are available (12) on the thallium ion-induced chemical shifts of carbonyl carbon resonances of [(1- ^{13}C)D-Val 8]gramicidin A and [(1- ^{13}C)D-Leu 14]gramicidin A, which are included as the X's in Fig. 4B. While not helically equivalent to L-residue carbonyls, these D-residue carbonyls are helically equivalent to each other and are also susceptible to ion-induced chemical shifts, which must be consistent with the L-residue data as to location but not as to sign and magnitude. The D-residue data are not consistent with the L-residue data for the parallel double-stranded structure (Fig. 4B). Thus, the double-stranded helices are not the channel state of interest.

In Fig. 4C the data of Fig. 3, A through H, are plotted for the single-stranded β -helix. In this case, two symmetrically related binding sites are observed, as required by the symmetric single-channel current-voltage curves (30, 31), as required by the previous demonstration of two binding constants (the difference between the tight and weak binding constants being repulsion between ions on double occupancy) (27), and as required by the exposure of the ethanolamine end to the aqueous interface and by the buried formyl end [demonstrated in (10) and by Fig. 3, I and J].

In addition, ion-induced carbonyl carbon chemical shifts can be used to determine helical sense of the single-stranded structure. This has been done with [(1- ^{13}C)D-Val 8]gramicidin A and [(1- ^{13}C)D-Leu 14]gramicidin A (12). Examination of the structure of the single-stranded helix shows that for the left-handed helix the residue 14 carbonyl is in the binding-site segment of the channel, whereas the residue 8 carbonyl is well removed from the binding site segment (Fig. 4C). For the right-handed single-stranded β -helix, the reverse is the case; the residue 8

carbonyl carbon is at the center of the binding site segment, and the residue 14 carbonyl is well removed from the segment. The observed thallium ion-induced chemical shifts for residues 8 and 14 are also included as X's in Fig. 4C, where they are correct for the left-handed helical sense.

Thus, ion-induced carbonyl carbon chemical shifts have provided a complete resolution of the issue of the single-versus double-stranded helix for the channel state of gramicidin A and have determined the helical sense. It should be emphasized that this is the description of the major ion-conducting state of gramicidin in lipid bilayers and in no way counters the excellent solution and solid-state studies of polymerized L-D structures, including the gramicidins, which can occur in the double-stranded helical state.

DAN W. URRY
TINA L. TRAPANE
KARI U. PRASAD

Laboratory of Molecular Biophysics,
University of Alabama School of
Medicine, Birmingham 35294

References and Notes

- H.-J. Apell, E. Bamberg, H. Alpes, *J. Membr. Biol.* **31**, 171 (1977).
- E. Bamberg and P. Läuger, *ibid.* **11**, 177 (1973).
- H.-A. Kolb, E. Bamberg, P. Läuger, *ibid.* **20**, 133 (1975).
- H. P. Zingsheim and E. Neher, *Biophys. Chem.* **2**, 197 (1974).
- W. R. Veatch, R. Mathies, M. Eisenberg, L. Stryer, *J. Mol. Biol.* **99**, 75 (1975).
- D. W. Urry, M. C. Goodall, J. D. Glickson, D. F. Mayers, *Proc. Natl. Acad. Sci. U.S.A.* **68**, 1907 (1971).
- Yu. A. Ovchinnikov and V. T. Ivanov, in *Con-*

formation in Biology, R. Srinivasan and R. H. Sarma, Eds. (Adenine, New York, 1982), pp. 155-174.

- S. V. Sychev and V. T. Ivanov, in *Membranes and Transport*, A. N. Martonosi, Ed. (Plenum, New York, 1982), vol. 2, pp. 301-307.
- F. Heitz, B. Lotz, G. Detriche, G. Spach, *Biochim. Biophys. Acta* **596**, 137 (1980).
- S. Weinstein, B. A. Wallace, E. R. Blout, J. S. Morrow, W. Veatch, *Proc. Natl. Acad. Sci. U.S.A.* **76**, 4230 (1979).
- D. W. Urry, K. U. Prasad, T. L. Trapane, *ibid.* **79**, 390 (1982).
- D. W. Urry, J. T. Walker, T. L. Trapane, *J. Membr. Biol.* **69**, 225 (1982).
- E. Bamberg, H.-J. Apell, H. Alpes, *Proc. Natl. Acad. Sci. U.S.A.* **74**, 2402 (1977).
- R. Sarges and B. Witkop, *J. Am. Chem. Soc.* **86**, 1862 (1964).
- K. U. Prasad, T. L. Trapane, D. Busath, G. Szabo, D. W. Urry, *Int. J. Pept. Protein Res.* **19**, 162 (1982).
- D. W. Urry, T. L. Trapane, S. Romanowski, R. J. Bradley, K. U. Prasad, *ibid.* **21**, 16 (1983).
- D. W. Urry, A. Spisni, M. A. Khaled, *Biochem. Biophys. Res. Commun.* **88**, 940 (1979).
- I. Pasquali-Ronchetti, A. Spisni, E. Casali, L. Masotti, D. W. Urry, *Biosci. Rep.* **3**, 127 (1983).
- D. W. Urry, A. Spisni, M. A. Khaled, M. M. Long, L. Masotti, *Int. J. Quantum Chem. Symp. No. 6* (1979), p. 289.
- D. McBride and G. Szabo, *Biophys. J.* **21**, A25 (1978).
- E. Neher, *Biochim. Biophys. Acta* **401**, 540 (1975).
- D. W. Urry, C. M. Venkatachalam, A. Spisni, R. J. Bradley, T. L. Trapane, K. U. Prasad, *J. Membr. Biol.* **55**, 29 (1980).
- E. Bamberg and P. Läuger, *Biochim. Biophys. Acta* **367**, 127 (1974).
- D. W. Urry, T. L. Trapane, J. T. Walker, K. U. Prasad, *J. Biol. Chem.* **257**, 6659 (1982).
- D. W. Urry, T. L. Trapane, K. U. Prasad, *Int. J. Quantum Chem. Symp. No. 9* (1982), p. 31.
- E. Bamberg and P. Läuger, *J. Membr. Biol.* **35**, 351 (1977).
- D. W. Urry, C. M. Venkatachalam, A. Spisni, P. Läuger, M. A. Khaled, *Proc. Natl. Acad. Sci. U.S.A.* **77**, 2028 (1980).
- L. Masotti, A. Spisni, D. W. Urry, *Cell Biophys.* **2**, 241 (1980).
- B. A. Wallace, W. R. Veatch, E. R. Blout, *Biochemistry* **20**, 5754 (1974).
- D. W. Urry, in *The Enzymes of Biological Membranes*, A. N. Martonosi, Ed. (Plenum, New York, in press).
- D. Busath and G. Szabo, *Nature (London)* **294**, 371 (1981).
- Supported in part by NIH grant GM-26898.
- 22 March 1983

Abnormal Ion Permeation Through Cystic Fibrosis Respiratory Epithelium

Abstract. *The epithelium of nasal tissue excised from subjects with cystic fibrosis exhibited higher voltage and lower conductance than tissue from control subjects. Basal sodium ion absorption by cystic fibrosis and normal nasal epithelia equaled the short-circuit current and was amiloride-sensitive. Amiloride induced chloride ion secretion in normal but not cystic fibrosis tissue and consequently was more effective in inhibiting the short-circuit current in cystic fibrosis epithelia. Chloride ion-free solution induced a smaller hyperpolarization of cystic fibrosis tissue. The increased voltage and amiloride efficacy in cystic fibrosis reflect absorption of sodium ions across an epithelium that is relatively impermeable to chloride ions.*

Theoretical considerations (1) and experimental evidence (2) indicate that salt and water absorption are important in the regulation of the volume of liquid on the surface of proximal airways. A major driving force for volume absorption is active Na^+ transport by surface epithelial cells (2). This process is electrogenic [generates a transepithelial electric potential difference (PD)] and accounts for

most of the basal short-circuit current (I_{sc}) of epithelial preparations in vitro. Nasal and bronchial epithelia of subjects with cystic fibrosis (CF) are characterized in vivo by three abnormalities that reflect altered ion transport or permeability and may be linked to deranged surface liquid metabolism, thickened mucus, and recurrent pulmonary infection (3): (i) the basal transepithelial PD is